High-Throughput Glomeruli Analysis of μCT Kidney Images Using Tree Priors and Scalable Sparse Computation

Carlos Correa Shokiche[1,2(✉)], Philipp Baumann[3], Ruslan Hlushchuk[2], Valentin Djonov[2], and Mauricio Reyes[1(✉)]

[1] Institute for Surgical Technology and Biomechanics, University of Bern, Bern, Switzerland
{carlos.correa,mauricio.reyes}@istb.unibe.ch
[2] Institute of Anatomy, University of Bern, Bern, Switzerland
[3] Department of Business Administration, University of Bern, Bern, Switzerland

Abstract. Kidney-related diseases have incrementally become one major cause of death. Glomeruli are the physiological units in the kidney responsible for the blood filtration. Therefore, their statistics including number and volume, directly describe the efficiency and health state of the kidney. Stereology is the current quantification method relying on histological sectioning, sampling and further 2D analysis, being laborious and sample destructive. New micro-Computed Tomography (μCT) imaging protocols resolute structures down to capillary level. However large-scale glomeruli analysis remains challenging due to object identifiability, allotted memory resources and computational time. We present a methodology for high-throughput glomeruli analysis that incorporates physiological *apriori* information relating the kidney vasculature with estimates of glomeruli counts. We propose an effective sampling strategy that exploits scalable sparse segmentation of kidney regions for refined estimates of both glomeruli count and volume. We evaluated the proposed approach on a database of μCT datasets yielding a comparable segmentation accuracy as an exhaustive supervised learning method. Furthermore we show the ability of the proposed sampling strategy to result in improved estimates of glomeruli counts and volume without requiring a exhaustive segmentation of the μCT image. This approach can potentially be applied to analogous organizations, such as for example the quantification of alveoli in lungs.

1 Introduction

Kidney-related diseases have incrementally become an important public health issue worldwide. According to the International Federation of Kidney Foundation, chronic kidney disease is an important cause of death. Yet the underpinning mechanisms are still poorly understood. In general, the kidney is the organ responsible for urine production through filtration units called glomerulus. The statistics associated with glomeruli are crucial since they are in direct relation

S. Ourselin et al. (Eds.): MICCAI 2016, Part II, LNCS 9901, pp. 370–378, 2016.
DOI: 10.1007/978-3-319-46723-8_43

with the state, efficiency and filtration power of the kidney. However, the current standard for quantification of these structures relies on stereology, which involves a very time-consuming and costly manual analysis of each histological section, and therefore is not carried out by most laboratories.

In the last years, due to further development of micro-Computed Tomography (μCT), it is possible to resolute structures down to capillary level. Supervised machine learning algorithms have been used to tackle the automation task of the quantification process. Rempfler [11] and Schneider [12] performed image segmentation based on supervised random forest (RF) with vessel completion under physiological constrains for brain networks. However, the segmentation task in general remains challenging due to large scale datasets with scarce labelled data for model training, as well as a poor distinction between glomeruli and other structures such as capillaries.

We propose an efficient approach for large-scale glomeruli analysis of μCT kidney images exploiting physiological information. The key idea is to model the relationship between the kidney vasculature topology and the glomeruli counts. This relationship is based on the allometry (i.e. proportions) between parental and children vessel radii along the vascular tree, allowing us to derive glomeruli count bounds. This bound serves as initialisation of an iterative sampling strategy that incrementally updates estimates of the glomeruli number and their total volume. The update step proceeds on selected regions with semi-supervised segmentation, which relies on sparse-reduced computation [1], suitable for high-throughput data. We report results on a database of μCT kidney images, comparing it to an exhaustive RF-based segmentation method. We demonstrate the ability of the sparse sampling strategy to provide accurate estimates of glomeruli counts and volume at different levels of image coverage.

2 Methods

We first start with a brief description of the kidney morphology, followed by descriptions of the main steps depicted in Fig. 1.

Biological landmarks. The overall kidney structure consists of two large regions: medulla and cortex. Only within the latter glomeruli are uniformly distributed [3]. The natural boundary between those two regions is roughly delineated by the vascular tree. In turn, the kidney vasculature consists of two trees (i.e. arterial and venal tree) connected in series, where the joining points correspond to the glomeruli. For glomeruli analysis, the arterial tree is of interest [3].

Preprocessing: Vasculature tree separation. As only a coarse description of the vasculature tree is necessary, simple thresholding and connected component analysis were adopted in this study, and resulted in an effective and practical solution. We observed that downsampling the image (by a factor of 8 per axis) does not affect the main topological features, since we are interested only in the split proportions between main large branches, while providing a computationally efficient solution.

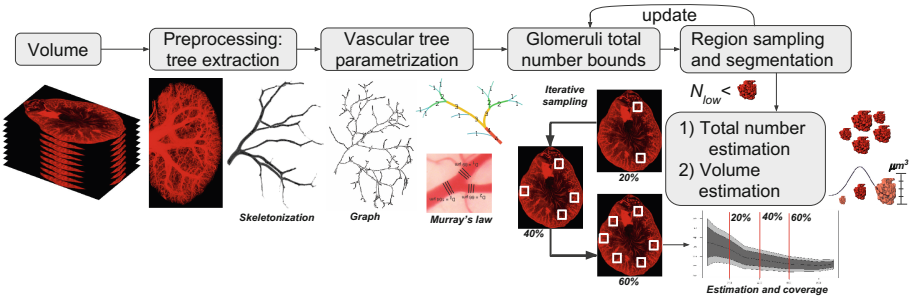

Fig. 1. Main steps of the proposed pipeline: from the raw image, physiological relations of the kidney vasculature are extracted, serving as inputs for an estimation of counting bounds. These are then updated by segmentation within an iterative sampling scheme resulting in new glomeruli count and total volume estimates.

Vascular tree parametrization and medulla extraction. The input image is skeletonized by a 3D medial axis thinning algorithm. From the skeleton, a graph is constructed using Kerschnitzki's approach [8]. The leaves (i.e. terminal nodes) of the graph serve as landmarks of the boundary between cortex and medulla. Hence, they are used as point cloud for a convex hull that partitions the kidney into medulla and cortex regions. This reduces the search space to about 60 % of the total kidney volume. In the next step, we will show how the obtained vascular tree parameterization is used to derive bounds for glomeruli counts.

Deriving bounds for glomerular counts. Following the minimum work principle [9,10], Murray's law relates the children branch radii with their parental branch radius, as $r_p^\gamma = r_{c_1}^\gamma + r_{c_2}^\gamma$ with $\gamma = 3$, where r_p denotes the radius of the parental branch and r_{c_i} the i-th child branch radius. Sherman [13] reports a corresponding exponent value of 2.61 for arteries and 2.76 for veins. For our purposes we use a general version with $\gamma \in [2, \infty+)$, which allows for convexity. Without loss of generality, we reparametrise the radii relation into the analogue circle cross-sectional area $A = \pi r^2$. This parameterisation provides us with a robust estimation of the equivalent radii, because the area in the image is less prone to a chosen orientation than the radius. Straightforward calculations give the rule $A_p^{\gamma/2} = A_{c_1}^{\gamma/2} + A_{c_2}^{\gamma/2}$. Assuming a dense and symmetrical binary tree, we obtain by recursion the following relation between the parental and the K-th grand-child branches:

$$A_1^{\gamma/2} = \sum_{i=1}^{2^K} A_{i+2^K}^{\gamma/2} \quad \text{for} \quad K \in \mathbb{N}, A_i \in \mathbb{R}^+ , \tag{1}$$

where K refers to the depth of the tree, A_1 is the largest parental circular cross-sectional area and A_{i+2^K} is the i-th grand-child circular cross-sectional area at the K-th tree depth level. Under the identical and independent distributional normality assumption of circular cross-sectional area per K-th depth

level $A_{i+2^K} \sim \mathcal{N}(A_K, \sigma^2_{A_K})$, we have $\mathbb{E}[A_{i+2^K}] = A_K$. Applying linearity of the expectation operator $\mathbb{E}[\cdot]$ and Jensen's inequality for convex functions (hence the necessary condition $\gamma \in [2, \infty+)$) on Eq. (1), we obtain after simple calculations

$$N = 2^K \geq \mathbb{E}\left[A_1^{\gamma/2}\right] \cdot A_K^{-\gamma/2} \geq \left(\frac{A_I}{A_K}\right)^{\gamma/2}, \tag{2}$$

where K specifies the expected depth of the arterial tree and N the expected number of glomeruli for a tree with K depth level. Here A_K is the cross-sectional area at the K-th terminal level corresponding to the expected cross-sectional area of the entry capillary into the glomerulus and A_I denotes the expected cross-sectional area at the largest parental arterial vessel (i.e. $A_I > A_i > A_K > 0$).

Determining number of sampled regions for segmentation. Let us consider a fixed known partition of B regular regions and drawing b sample regions with equal inclusion probability [14]. In order to determine the number of sample regions, one can derive the required quantity from the bounded probability of an unbiased estimator for the total number of events $\hat{N} : \mathbb{P}\left(\frac{|\hat{N}-N|}{\sqrt{\mathbb{V}[\hat{N}]}} > z_{\alpha/2}\right) = \alpha$, where $\frac{|\hat{N}-N|}{\sqrt{\mathbb{V}[\hat{N}]}} \sim \mathcal{N}(0,1)$ for a desired confidence level α ($\alpha = 5\,\%$ as customary for statistical hypothesis testing). One specifies an absolute error d on the total number estimator (i.e. $z_{\alpha/2}\sqrt{\mathbb{V}[\hat{N}]} \leq d$), and then solving for b gives

$$b = \frac{1}{1/b_0 + 1/B}, \quad \text{where} \quad b_0 = \sigma^2 \left(\frac{B z_{\alpha/2}}{d}\right)^2, \tag{3}$$

where $\mathbb{V}[\cdot]$ denotes the variance operator, the hat notation ($\hat{\cdot}$) refers to estimators and σ^2 is the population variance of the total number, which can be obtained from previous studies or estimated from training data.

Scalable glomerular segmentation using sparse computation. Knowing the number of sampled regions b (Eq. (3)), uniform regions are extracted and segmented. In order to address the issue of scalability and the use of unlabelled data in large image volumes, we draw upon *sparse-reduced computation* (SRC) for efficient graph-partitioning introduced by Baumann et al. [1]. Sparse-reduced computation creates a compact graph representation of the data with minimal loss of relevant information. This is achieved by efficiently projecting the feature vectors onto a low-dimensional space using a sampling variant of principal component analysis. The low-dimensional space is then partitioned into grid blocks and feature vectors that fall into the same or neighbouring grid blocks are replaced by representatives. These representatives are computed as the center of mass of the feature vectors they represent. The graph is then constructed on the representatives rather than on the feature vectors which significantly reduces its size. The segmentation for the representatives is obtained by applying Hochbaum's normalized cut (HNC) [7], which can be solved in polynomial time while the normalized cut problem is NP-hard.

Iterative count refinement: unbiased estimators for total number and total volume of glomeruli. We can iteratively refine our estimates by including more segmented subvolumes b as a function of a target confidence of the glomeruli counts and volume estimates. To this end, in this study we adopted a bootstrapping replication scheme [6]. Based on unbiased estimators for totals with equal inclusion probabilities with uniform random sampling without replacement [14], we obtain for each j-th replication

$$\hat{N}_j = B\bar{y}_{bj} = \frac{B}{b}\sum_{i}^{b} y_{ij} \quad \text{and} \quad \hat{V}_j = B\bar{v}_{bj} = \frac{B}{b}\sum_{i}^{b} v_{ij} \quad \forall j \in J \quad (4)$$

$$\hat{\mathbb{V}}[\hat{N}_j] = B^2\hat{\mathbb{V}}[\bar{y}_{bj}] = B(B-b)\frac{s^2_{\hat{N}j}}{b} \quad \text{and} \quad \hat{\mathbb{V}}[\hat{V}_j] = B^2\hat{\mathbb{V}}[\bar{v}_{bj}] = B(B-b)\frac{s^2_{\hat{V}j}}{b},$$

where $\hat{N}_j$ and $\hat{V}_j$ are unbiased estimators for total glomerular number and volume, respectively. y_i and v_i are the actual glomeruli counts and the segmented volume, both on the i-th segmented region. Empirical booststrap distributions are generated from J estimate replications, which are drawn with replacement, and hence confidence intervals are constructed for the mean number $\hat{\bar{N}}$ and mean total volume $\hat{\bar{V}}$ estimators, in order to assess their quality in terms of their statistical consistency: unbiasedness and low variability.

3 Results

Data source and experiments. Our database consisted of 9 right kidneys belonging to two groups: 5 healthy mice and 4 GDNF+/− mice, which are genetically modified, and known to have about 30 % fewer glomeruli and smaller kidney volume [4,5]. The volume size ranges from $1\,\mathrm{K} \times 2.5\,\mathrm{K} \times 4\,\mathrm{K}$ up to $3\,\mathrm{K} \times 4\,\mathrm{K} \times 6\,\mathrm{K}$ voxels, which corresponds to 30–80 GB. The isotropic size of a voxel is $2.6\,\mu\mathrm{m}$. We performed two experiments: (1) Evaluation of the sparse-reduced semi-supervised segmentation, (2) Evaluation of the iterative sampling scheme. In experiment (1) we generated ground-truth by manually annotating a reduced region of interest of size $512 \times 512 \times 141$ and compared the sparse-reduced semi-supervised segmentation to an exhaustive RF segmentation.

Experiment 1. We evaluated the performance of sparse-reduced computation with different grid resolutions. Figure 2 illustrates the process of sparse-reduced computation for a manually segmented region which comprises 36 million voxels. Rather than constructing a complete graph with 36 million nodes, the sparse-reduced computation approach constructs a much smaller graph by consolidating highly-similar voxels into a small number of representatives. The reduced graph contains a node for each representative. The segmentation for the representatives is obtained by applying Hochbaum's normalized cut (HNC) [7] to the reduced graph formed by edges connecting only representatives. The labels that are assigned to the representatives are passed on to each of the voxels that

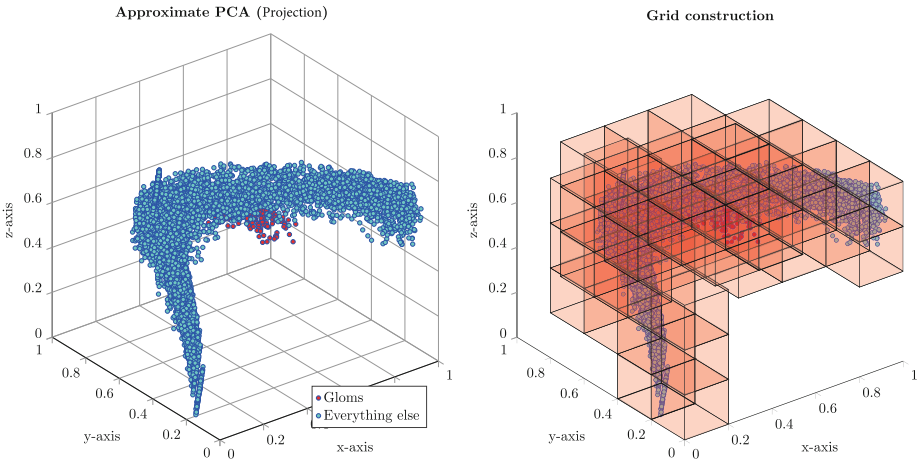

Fig. 2. Sparse-reduced computation for semi-supervised segmentation. Left: Projection of feature vectors onto a 3-dimensional space. Right: Partitioning of 3-dimensional space into blocks and generation of representatives. Similarities are only computed between representatives of the same and neighboring blocks. This provides a significant reduction in computational complexity.

they represent. In this study, we used standard first and second order statistics intensity information as features (i.e. mean, quantiles, entropy, gradient, etc.).

We compared the sparse-reduced computation approach to an exhaustive RF based segmentation method [2] with 100 trees, depth = 18, and the same set of 19 features. In order to simplify the evaluations, no attempt to regularise the segmentation result was performed.

In Table 1 we report the overall performance for different grid resolutions in terms of accuracy, precision, recall, and F_1score. The grid resolution determines the number of divisions of each axis (e.g. 5 divisions per axis, cf. Fig. 2 right side), and hence it controls the total number of grid blocks. The results were compared with the exhaustive RF segmentation method. From Table 1 it is observed that higher grid resolutions yield better segmentation results, influencing most notably on accuracy and F_1score, up to a saturation point between grid size 10 and 15. In terms of computation load, the increase is negligible as the number of representatives is substantially low for all resolutions. In comparison to the exhaustive RF-based segmentation, the results are competitive and attractive in light of scenarios where labelled data and memory resources are limited.

Based on the results from this first experiment, we regarded the segmentation from the exhaustive RF-based method as a *silver* ground-truth to evaluate in experiment 2 the reliability of the iterative sampling scheme. The RF segmentation was fully run on the 9 datasets and then a visual inspection was performed for *sanity* check. Minimal manual corrections were needed.

Table 1. Segmentation performance of sparse-reduced computation at different grid resolutions, and RF-based segmentation. Best results of SRC are in bold.

Experiment	Accuracy	Precision	Recall	F_1score
Sparse - grid resolution 5	0.9829	**0.736**	0.284	0.41
Sparse - grid resolution 10	0.9858	0.618	**0.843**	**0.713**
Sparse - grid resolution 15	**0.9864**	0.661	0.719	0.689
Sparse - grid resolution 20	0.985	0.664	0.576	0.617
Exhaustive random forest	0.99	0.761	0.793	0.777

Experiment 2. In this experiment we are interested in evaluating the unbiasedness (consistency) and efficiency of both glomeruli count and total volume estimators for different number of segmented sampled regions, reformulated as kidney volume coverage from 5 % up to 80 %. We considered $J = 10$ bootstrap replications in order to derive bootstrap empirical distributions and construct bootstrap confidence intervals for the mean estimators. Figure 3(a)–(b) show the decrease in the total volume and count errors as more volume is covered, with values ranging from 6 % down to 1 % for volume and count error. This is consistent with the unbiasedness property of the estimators. Furthermore, it also shows an increase in efficiency, depicted by the reduction of the estimator variance as larger volume is covered.

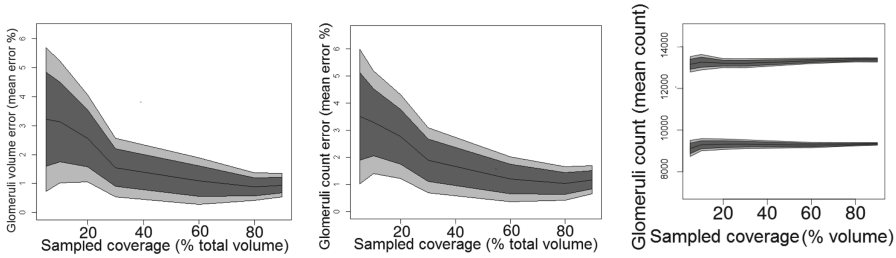

(a) Error on glomeruli total volume (%)

(b) Error on glomeruli total count (%)

(c) Glomeruli total counts per group

Fig. 3. Iterative sampling scheme: performance of mean total and mean total volume estimators as a function of volume coverage for the complete 9 datasets (a)–(b), and mean total counts per group (c): healthy and genetically modified GDNF+−. The central solid line corresponds to the mean estimation. Confidence intervals at levels $\alpha = 0.05$ and $\alpha = 0.2$ are shown as shaded areas.

Figure 3(c) depicts that the mean total count estimate separates into the healthy and the genetically modified GDNF+− groups. We identify the nearly 30 % mean difference in total glomeruli number, as reported in the literature [4,5]. Note that the bootstrap confidence intervals for the mean total count

estimator do not overlap between groups, which suggests that the statistical efficiency (i.e. low variance) of the estimator allows researchers to discriminate groups in studies involving GDNF+− subjects, as disease model.

4 Discussion and Conclusion

In this study we have presented a fast and efficient iterative sampling strategy to quantify glomeruli in large μCT kidney images. In contrast to previous approaches, we combine estimators of volume and counts with a scalable and computationally efficient semi-supervised segmentation approach. The proposed pipeline exploits physiological relations of kidney vasculature and glomeruli counts and volume, and yields fast and statistically efficient estimators with accurate estimates of them. The iterative nature of the approach allows users to define a trade-off between accuracy of the estimations and computational complexity, up to a desired level. The sparse-reduced computation is suitable for large image volumes for which annotated data is typically scarcely available, while yielding competitive results with standard supervised RF-based segmentation approaches. The method features high scalability through an efficient computation of similarities among representatives. The proposed approach can be extended for high-throughput analysis of structures in large-scale images. Also it can potentially be applied to analogous organizations, such as for example the quantification of alveoli in lungs.

Acknowledgements. This work is funded by the Kommission für Technologie und Innovation (KTI) Project No. 14055.1 PFIW-IW.

References

1. Baumann, P., et al.: Sparse-reduced computation - enabling mining of massively-large data sets. In: Proceedings of ICPRAM 2016, pp. 224–231 (2016)
2. Breiman, L.: Random forests. Mach. Learn. **45**(1), 5–32 (2001)
3. Bruce, M., et al.: Berne and Levy physiology, 6th edn. Elsevier (2010)
4. Cullen-McEwen, L., Drago, J., Bertram, J.: Nephron endowment in glial cell line-derived neurotrophic factor (GDNF) heterozygous mice. Kidney Int. **60**(1), 31–36 (2001)
5. Cullen-McEwen, L., et al.: Nephron number, renal function, and arterial pressure in aged GDNF heterozygous mice. Hypertension **41**(2), 335–40 (2003)
6. Davison, A., Hinkley, D.: Bootstrap Methods and their Applications. Cambridge University Press, Cambridge (1997)
7. Hochbaum, D.: Polynomial time algorithms for ratio regions and a variant of normalized cut. IEEE Trans. Pattern Anal. Mach. Intel. **32**, 889–898 (2010)
8. Kerschnitzki, M., et al.: Architecture of the osteocyte network correlates with bone material quality. J. Bone Miner. Res. **28**(8), 1837–1845 (2013)
9. Murray, C.: The physiological principle of minimum work: II. Oxygen exchange in capillaries. Proc. National Acad. Sci. United States Am. **12**(5), 299–304 (1926)
10. Murray, C.: The physiological principle of minimum work: I. the vascular system and the cost of blood volume. Proc. Natl. Acad. Sci. U.S.A. **12**(3), 207–214 (1926)

11. Rempfler, M., et al.: Reconstructing cerebrovascular networks under local physiological constraints by integer programming. Med. Image Anal. **25**(1), 86–94 (2015). special Issue on MICCAI 2014
12. Schneider, M., et al.: Tissue metabolism driven arterial tree generation. Med. Image Anal. **16**(7), 1397–1414 (2012). special Issue on MICCAI 2011
13. Sherman, T.: On connecting large vessels to small. the meaning of murray's law. J. Gen. Physiol. **78**(4), 431–453 (1981)
14. Thompson, S.: Sampling. Wiley series in probability and statistics. Wiley (2002)